Variational study of mesh and shape optimization

Alain Dervieux, Frédéric Alauzet, Didier Chargy

Variational study of mesh and shape optimization

Alain Dervieux[0000−0002−3936−3285] and
Frédéric Alauzet[0000−0002−8025−3862] and
Didier Chargy

Abstract This paper focuses on the combination of design optimization with anisotropic mesh adaptation. The key components are: unstructured mesh for CFD, use of adjoint state for design, use of metric-based mesh adaptation.

1 Motivations

In order to design the new transport devices answering to the climatic challenge, the needs in High-Fidelity CFD simulation are increasing. High-Fidelity CFD simulation demands:
- high-fidelity models like RANS and hybrid RANS/LES,
- high-fidelity approximations with a strong control of the approximation error.

This paper focuses on the combination of design with anisotropic mesh adaptation. The key components are: unstructured mesh for CFD, use of adjoint state for design, use of mesh adaptation.

The adjoint state was popularized by J.L. Lions in his book "Optimal Control" [5] in 60's. It was demonstrated by O. Pironneau for CFD design based on the Full Potential model [7] and then by A. Jameson [4] for the Euler model. Unstructured-mesh CFD was strongly supported and developed in France by Dassault Aviation (J. Périaux, P. Perrier, program HERMES). Adjoint methods use intensively code differentiation, strongly supported in France by Dassault Aviation (J. Périaux, B.

Alain Dervieux
Lemma, Biot, France, and Univ. Côte d'Azur/INRIA Projet Ecuador, Sophia-Antipolis, France, e-mail: alain.dervieux@inria.fr

Frédéric Alauzet
GammaO, Équipe INRIA-ONERA-Centre INRIA de Saclay, Univ. Paris-Saclay, Palaiseau, France and Lemma, Biot, France e-mail: frederic.alauzet@inria.fr

Didier Chargy
Lemma, Biot, France e-mail: didier.chargy@lemma-ing.com

Stoufflet, program GENIE). A cooperation on metric-based mesh adaptation started very early between INRIA, Paris 6 and Dassault (J. Périaux, B. Stoufflet).

It appears today that with the new algorithms for mesh adaptation, new efficient and accurate automatical tools are available for maximizing the quality of high-fidelity prediction. The advantages of these tools will probably in the near future make their use mandatory in the industrial practice. Automatic tools are already available for design optimization. Today these tools rely on a generation of non-adaptative or poorly adaptative CFD. It is then important to propose for the very near future a composite algorithm which combines in best conditions the novel mesh adaptation technology with most recent or novel design optimization loops.

The first part of this paper gives some state-of-the-art of the anisotropic goal-oriented mesh adaptation algorithms. The second part examines the integration of these algorithms in a design loop.

2 Anisotropic mesh adaptation

The ingredients of anisotropic mesh adaptation are in short:
- Spalart-Allmaras RANS and DDES vertex-centered FEM-FVM using tetrahedra,
- anisotropic metric-based local remesher.

They are described and discussed in details in [1, 2]. The Goal Oriented (GO) version minimizes the error on a prescribed scalar output. The error analysis relies on an adjoint state. The double loop mesh adaptation algorithm (Figure 1) contains an *inner loop* which iteratively adapts the mesh and recomputes the flow, the adaptation being performed while maintaining the total number of nodes in the mesh. The double loop mesh adaptation algorithm contains also an *outer loop* of refinement, that is responsible of increasing the total number of nodes in such a way that the double loop organizes the convergence of the discrete solution to the exact one.

2.1 Earlier higher-order convergence and important details of flow

Anisotropic adaptation results in *earlier* high-order convergence.
We illustrate this fact with a case of the AIAA High Lift Prediction Workshop [11], see Figure 2. In the right figure, the convergence of the lift coefficicent is depicted. Five red square show different calculations with best practice meshes composed of 205 M nodes. An confidence interval $[C_L = 2.365 \pm 0.05]$ is then derived. Six blue stars are also depicted, produced by the application of the GO mesh adaptation double loop (values of lift at end of outer loops). We observe that meshes with 2.73M, 5.41M, 10.5M, 20.0M nodes of the process produce lift predictions inside the confidence interval, showing an accuracy comparable to the accuracy of the five 205 M nodes computations. Since adjoint-based/GO approaches are designed to

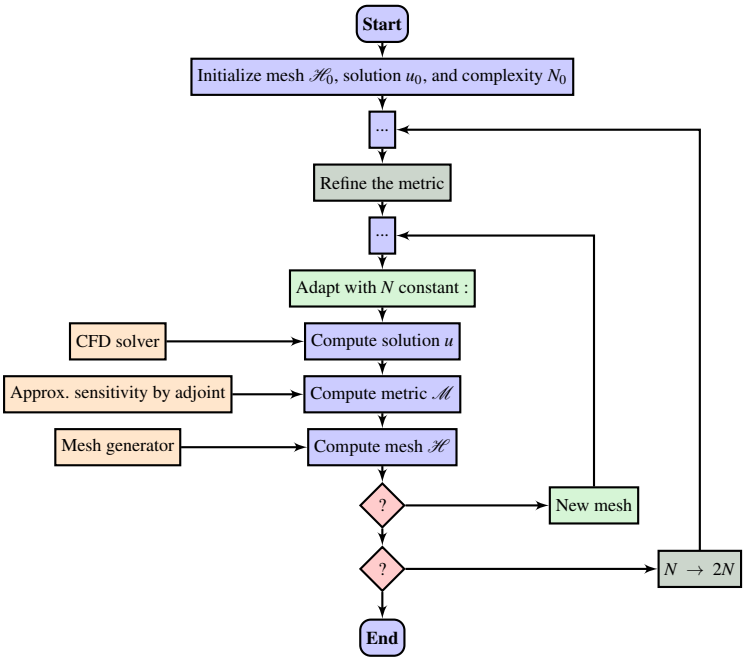

Fig. 1 Anisotropic double loop GO mesh adaptation

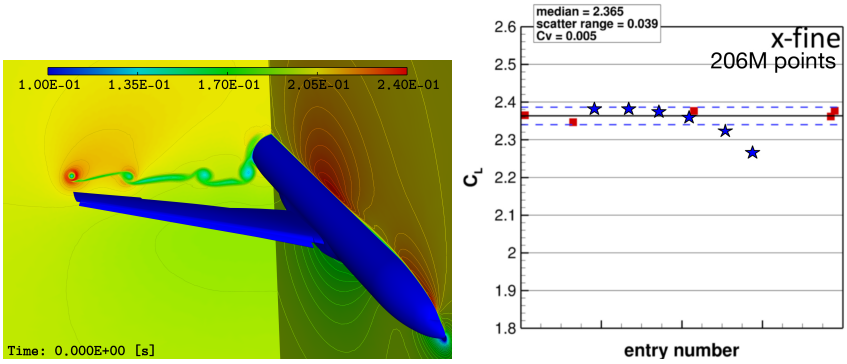

Fig. 2 High-Lift workshop. *Left*: GO adaptation with lift as functional. Local Mach number, 5.41M cells. *Right*: Lift predictions against different computations. ■: five computation with the workshop mesh of 206M cells. ★(right to left) are produced by a GO adaptation loop with lift as functional, successive meshes of (right to left) 0.68M, 1.35M, 2.73M, 5.41M, 10.5M, and 20.0M nodes.

find the mesh which minimizes the error on the target scalar output, this method *concentrate mesh in regions which are important for the output accuracy*. This is illustrated by pictures from the above computation (Figure 3).

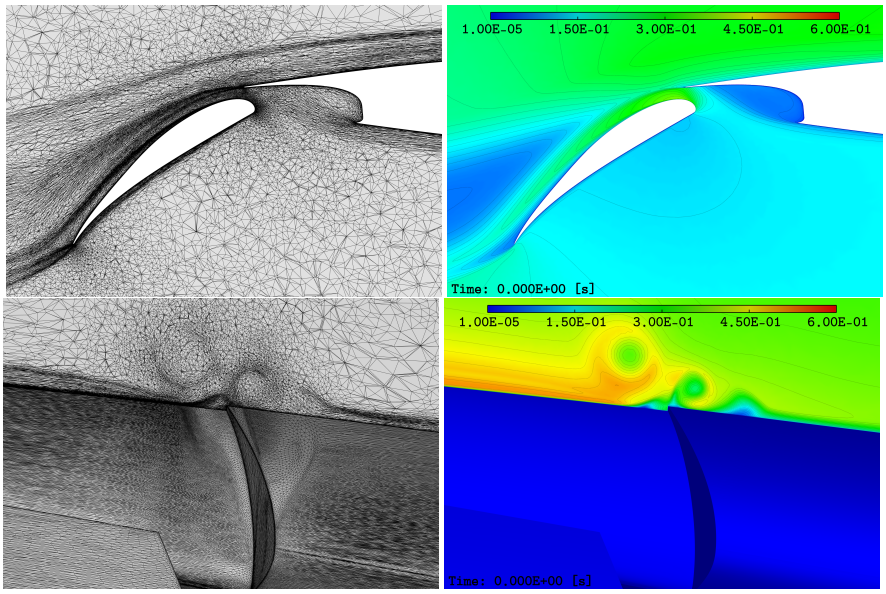

Fig. 3 Same High-Lift workshop calculation, adapted mesh composed of 5.41M cells and the associated solution (local Mach number).

2.2 GO meshes can produce much better results than Taylored finer meshes

This statement is illustrated by computations from the 2nd AIAA Sonic-Boom Prediction Workshop, [8]. The geometry, depicted in Figure 4, is a shape for a supersonic aircraft with mitigated sonic boom. The pressure perturbation is measured in a horizontal plane at some distance under the aircraft. A non-adapted and an adapted calculation have been performed with a post-processing [10] showing the local error (black vertical intervals). It appears that the computation with a 13M nodes taylored mesh (aligned with main shock direction) still show large local errors. In contrast, the GO approach with 5.9 M nodes shows small error intervals almost everywhere (Figure 5).

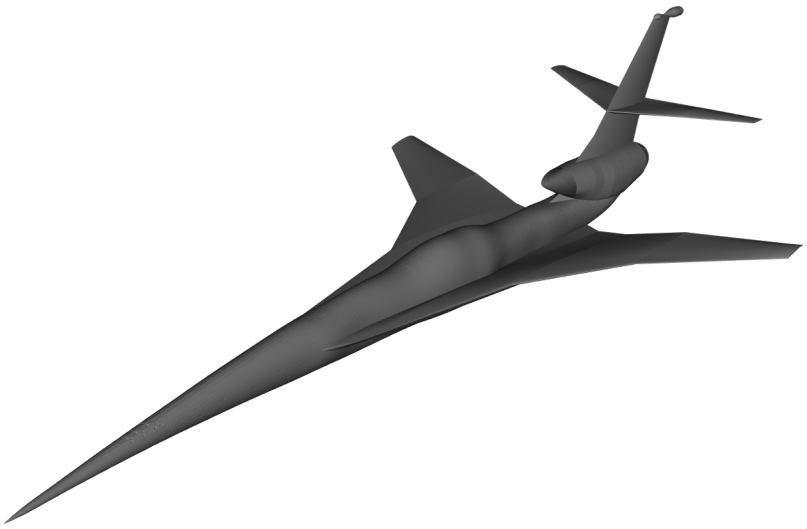

Fig. 4 13M Taylored mesh $dp/pinf$ (left) vs 5.9 M adapted mesh $dp/pinf$ (right). Black vertical intervals are estimates of local approximation uncertainty.

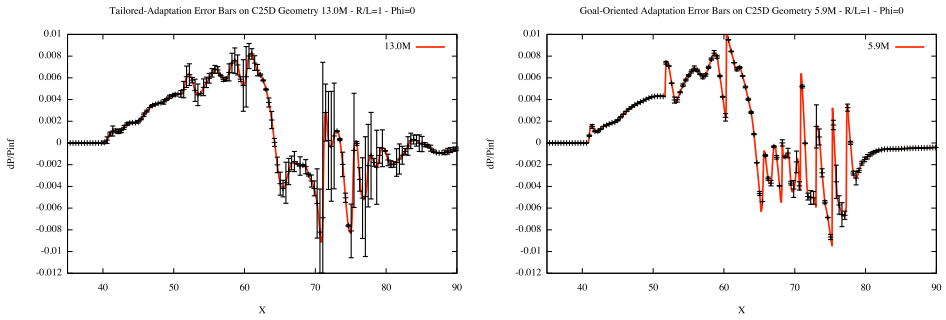

Fig. 5 13M Taylored mesh $dp/pinf$ (left) vs 5.9 M adapted mesh $dp/pinf$ (right). Black vertical intervals are estimates of local approximation uncertainty.

2.3 Some remarks on the Goal-Oriented adaptation

As illustrated in Figure 2, a rather neat convergence of the *functional* is obtained. We emphasize that the GO algorithm does *not* provide a mesh-converged *flow*. Indeed, the error which is minimized is weighted by the derivative of the adjoint state. For example, regions where adjoint is constant are not refined.

Further, the GO algorithm relies on an adjoint flow while *not* having any evident mechanism for ensuring that the mesh is sufficient for computing this *adjoint flow*.

3 Mesh adaptation for design

Let us make precise the kind of tool we are developing. We focus on the *last phase* of design:
- main characteristics of the shape are chosen, defining the initial shape,
- an initial flow is computed as accurately as possible on this initial shape with GO mesh adaptation, maximizing the accuracy on the functional, for example the drag,
- it remains to slightly modify the shape in order to get the *last attainable improvements by design*.
The central question is:

How to continue towards drag minimization while still enjoying the accuracy of mesh adaptation.

3.1 Theoretical issues in mesh adaptation for design

3.1.1 Single adjoint approach

It is remarkable that:
- the GO adjoint state W^* computed for minimizing the *error* δj *on the functional* j w.r.t. metric $\mathscr{M}$ and,
- the design adjoint state for minimizing the functional j itself w.r.t. shape parameter γ_h,
are strictly the same:

$$\begin{aligned} \min_{\mathscr{M}} |j - j_h| \quad &\Rightarrow \quad W^* \\ \min_{\gamma_h} j_h \quad &\Rightarrow \quad W^* \end{aligned}$$

It is then natural to combine the two minimization loops using the same adjoint. This *single-adjoint* strategy will be illustrated in the numerical examples.

3.2 Double adjoint approach

The purpose of the design is to approximate the continuous optimal shape γ_{opt}.

$$\gamma_{opt} = Arg \min_{\gamma} j.$$

Then a more rational mesh adaptation criterion should concentrate on the accuracy for the optimal parameter:

Find a metric $\mathscr{M}_{opt}$ *and an approximate optimal shape* $\gamma_{opt,h}$

$$\gamma_{opt,h} = Arg \min_{\gamma_h} j_{(h)}.$$

such that the deviation $||\gamma_{opt,h} - \gamma_{opt}||$ *is minimized (in some norm):*

$$\min_{\mathscr{M}} ||\gamma_{opt,h} - \gamma_{opt}||.\square$$

In the above statement, index h holds for the discretization based on $\mathscr{M}_{opt}$. To address that latter problem, Becker *et al.* [9] proposed the following analysis:

$$0 = j'(\gamma_{opt}) - j'_h(\gamma_{opt,h}) = j'(\gamma_{opt}) - j'_h(\gamma_{opt}) + j'_h(\gamma_{opt}) - j'_h(\gamma_{opt,h}).$$

Thus:

$$j'_h(\gamma_{opt}) - j'_h(\gamma_{opt,h}) = j'_h(\gamma_{opt}) - j'(\gamma_{opt}).$$

Now:

$$j'_h(\gamma_{opt}) - j'_h(\gamma_{opt,h}) = j_h"(\gamma_{opt})(\gamma_{opt} - \gamma_{opt,h}) + R = j_h"(\gamma_{opt,h})(\gamma_{opt} - \gamma_{opt,h}) + R'.$$

Then:

$$\gamma_{opt} - \gamma_{opt,h} \approx \left[j_h"(\gamma_{opt})\right]^{-1} \Big(j'_h(\gamma_{opt}) - j'(\gamma_{opt}) \Big). \tag{1}$$

Then Becker *et al.* [9] propose to simplify the square Hessian matrix $j_h"(\gamma_{opt})$ by a scalar number times Identity. In fact, using Automatic Differentiation for example, the Hessian matrix $j_h"(\gamma_{opt})$ is certainly complex but not impossible to evaluate. Instead, let us simplify the initial minimal norm problem into the following Goal Oriented formulation:

$$\text{Minimize the error on} \quad (g_0, \gamma_{opt} - \gamma_{opt,h}).$$

We simplify it further by putting:

$$g = \left[j_h"(\gamma_{opt})\right] g_0$$

and analyzing the *GO minimization* of

$$(g\ ,\ j'_h(\gamma_{opt}) - j'(\gamma_{opt})) \equiv (g\ ,\ j'_h(\gamma_{opt}))$$

for an arbitrary g.
$\big(g\ ,\ j'_h(\gamma_h)\big)$ is a function θ_h of (γ_h, W_h, W_h^*):

$$\min_{\mathscr{M}} \ \theta_h\big(\gamma_h, W_h, W_h^*\big) \ \text{ under the constraint } \ K(\gamma_h, W_h, W_h^*) = 0$$

with $\theta_h\big(\gamma_h, W_h, W_h^*\big) = \Big(g\ , \Big(W_h^*, \frac{\partial \Psi_h}{\partial u}\big(\gamma_h, W_h\big)\Big) + \frac{\partial J_h}{\partial u}\big(\gamma_h, W_h\big)\Big)$ and where the *previous* state and adjoint state are the unknowns of a *new* state equation

$$K(\gamma_h, W_h, W_h^*) = 0$$

with:

$$K = (K_1, K_2)$$
$$K_1(\gamma_h, W_h, W_h^*) = \Psi_h(\gamma_h, W_h), \quad K_2(\gamma_h, W_h, W_h^*) = \frac{\partial \Psi_h}{\partial W_h}^*(\gamma_h, W_h) W_h^* + \frac{\partial J_h}{\partial W_h}(\gamma_h, W_h).$$

This time, the adaptation accounts for both state and adjoint flows local errors, weighted by a new adjoint $K'^{-1*}\partial\theta_h/\partial(W, W^*)$.

It remains to express the residuals K_1 and K_2 in terms of interpolation errors of state (W, W^*) in order to build a GO mesh adaptation loop for the optimal shape. □

The double-adjoint approach presented here does not take into account the constraints which are introduced on shape parameters in quasi all practical problems. Next section present an implementation of the single adjoint approach for which introducing constraints is trivial.

3.3 Implementation of single adjoint approach

In the last phase of industrial design, the shape optimization has to rely on:
- a sufficiently accurate *shape parametrization* in order to be able to get the best improvement,
- a highly accurate *simulation*, in order to better identify a local minimum,
- an accurate algorithm for searching the optimum.

We focus on the combination of:
- adjoint-based sensitivity to shape,
- Sequential Quadratic Programming for shape optimization, and
- anisotropic mesh adaptation for accurate functional evaluation.

An option would be to consider the mesh-adaptive solver as the solver to be installed inside the design loop. But the function which maps the *Shape* onto the *Mesh-adapted flow* is *not a differentiable mapping* due to the discontinuous changes in the underlying mesh performed by adaptation and SQP cannot be applied efficiently. It is possible to work on the coupling between SPQ and BFGS from one side with the adaptation. An example of this coupling for a simpler gradient loop as optimizer is discussed in [6]. In the present work, we install the double mesh-adaptation loop as an external loop with respect to the optimization loop. This is developed in Figure 6. Two applications are then presented.

3.4 Application to hydraulic design, 1, bulbous bow optimization

In this first example, the above loop is applied without the mesh adaptation sequence. This will permit to evaluate the efficiency of the association of SQP, shape

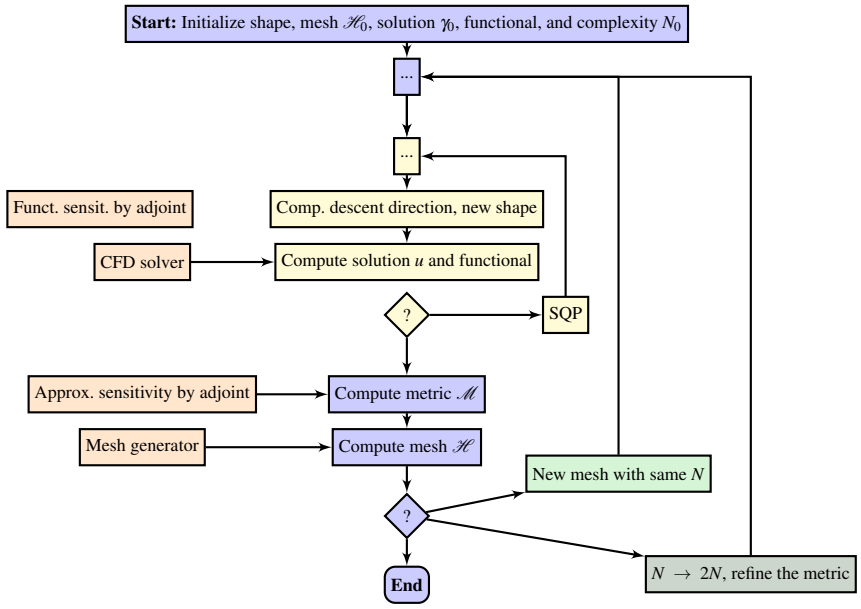

Fig. 6 Single-adjoint triple loop for adaptation, refinement and design

parametrization and volumic mesh deformation. We consider the well known David Taylor Model Basin 5415, a historical post-second war shape for a combattant ship, see the shape in Figure 7. We consider the optimization of the front bulb. The flow model involves the free surface. The mesh size is of 849709 nodes. An idea of the initial flow is given in Figure 8 in which are presented the free surface (indicated by the variation of fluid density) and the total pressure. Applying the SQP algorithm, we observe that with solely 5 SQP minimization iterations, this shape can be improved in such a way that the ship drag is reduced by 9%, Table 1. The modification of bulb shape (less flat at stagnation point) is slightly perceptible when examining the flow obtained at the end of optimization (Figure 9).

Fig. 7 Initial shape: David Taylor Model Basin 5415.

Mesh size	Optimization steps	Initial drag	Final drag
849709	5	10.9	10.1 (-9%)

Table 1 Optimisation of DTMB bulb.

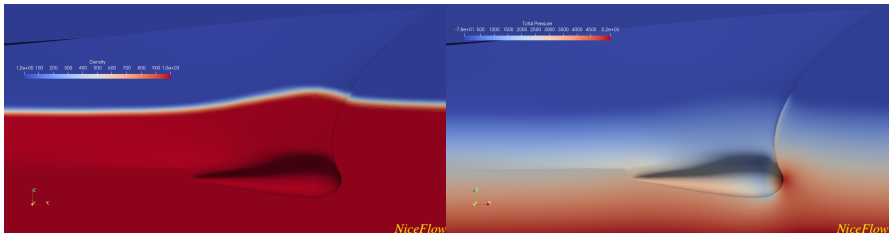

Fig. 8 David Taylor Model Basin 5415: density and pressure before optimization

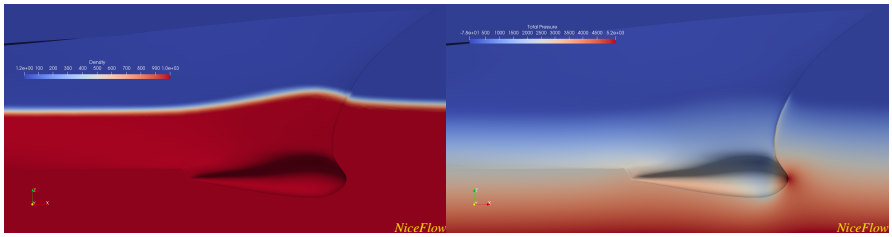

Fig. 9 David Taylor Model Basin 5415: density and pressure after optimization

3.5 Applications to hydraulic design, 2, VP1304 propeller

The last example combines mesh adaptation and shape optimization. The geometry is the ship VP1304 propeller model proposed by Postdam university and depicted in Figure 10. A first mesh adaptive double loop predicts accurately the flow, with a final mesh of 2.5M nodes. Then 100 shape degrees of freedom are introduced for optimizing the blades. Then the optimization process combined with mesh adaptation is started. The purpose is to increase the so-called *propeller efficiency*, ratio of propulsive power to absorbed power, which is then chosen as the scalar output, while the cost functional to minimize is chosen as the inverse of propeller efficicency. With this medium number of shape parameters, the combination of adaptation and optimization uses 20 mesh adaptations and a total of 80 SQP iterations. Inital and final meshes are shown in Figure 11. Initial and final flows are presented in Figure 12. Differences seem very small. The blades modifications are more evident, although not very large (Figure 13 and 14) This computation permitted to increase the propeller efficiency by 4.5%.

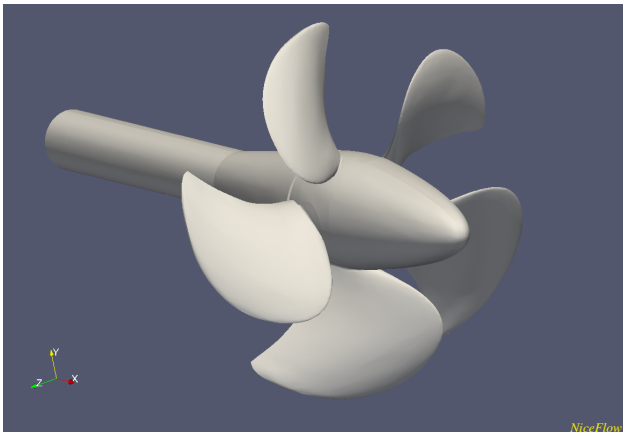

Fig. 10 VP1304 propeller: geometry

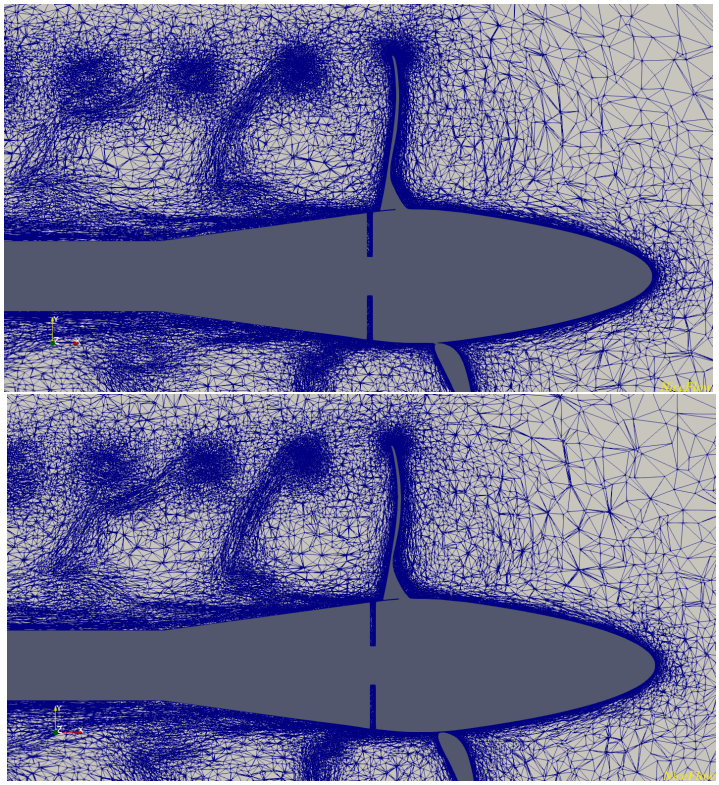

Fig. 11 VP1304 propeller: initial and final meshes

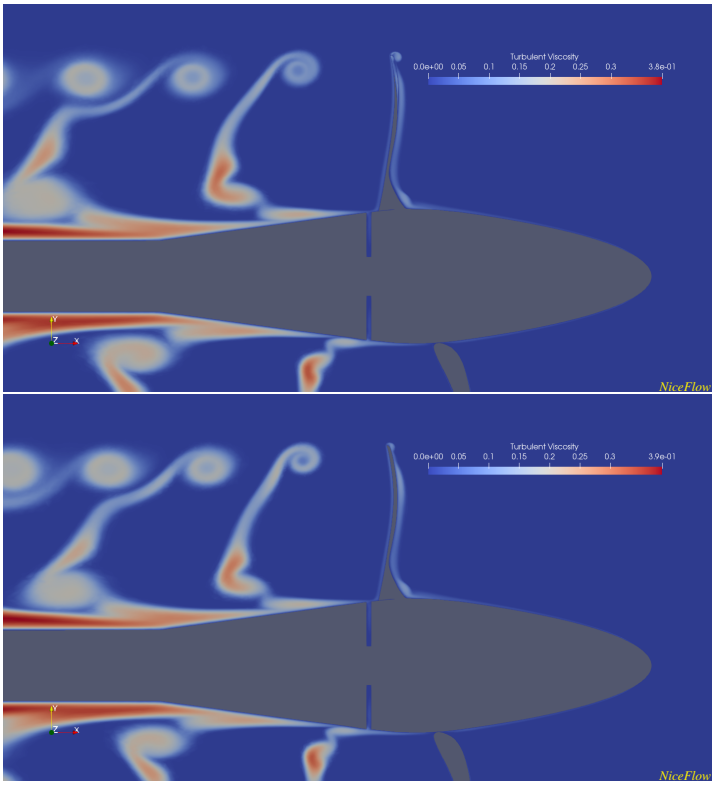

Fig. 12 VP1304 propeller: initial and final flows

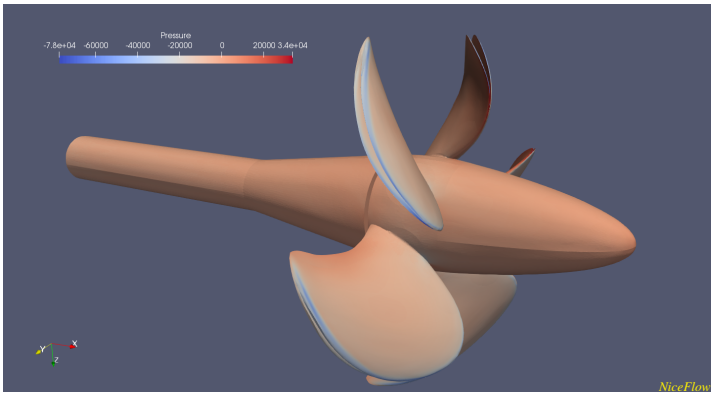

Fig. 13 VP1304 propeller: initial and final shapes

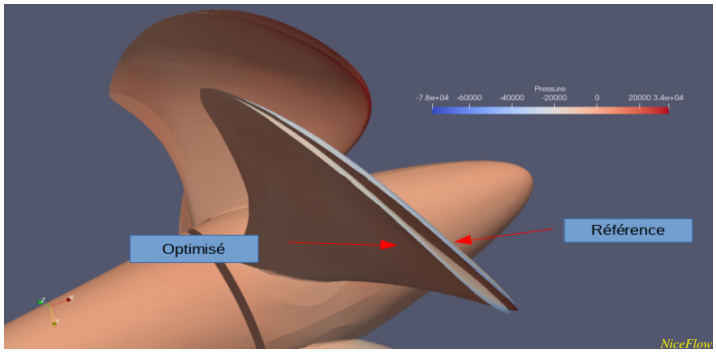

Fig. 14 VP1304 propeller: initial and final shapes

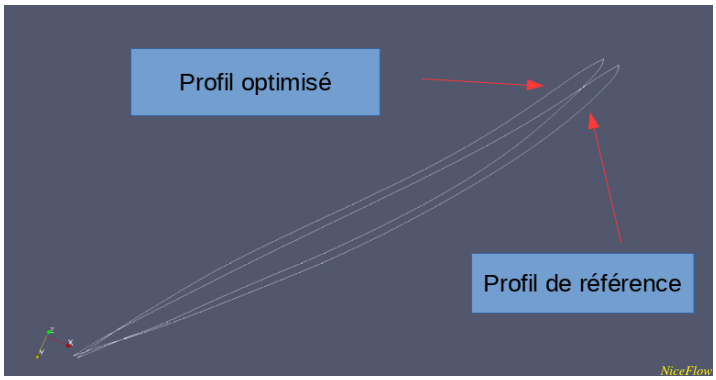

Fig. 15 VP1304 propeller: initial and final shapes

4 Concluding remarks

This short paper first shows that the new anisotropic mesh adaptation algorithms are efficient to get a more accurate and more efficicent solution. As concerns GO adaptation we observe that:
- a medium (3M) mesh GO-adaptation provides results that are equivalent to usual fine (200M) mesh computations.
- It results that when a massively parallel fine ($>$ 30M nodes) mesh GO-adaptation is available, the quality of the results will be hardly affordable when using a traditional non-adaptive approach.

These properties are important for initializing and performing a final design phase. Starting from a medium GO-adapted solution, the last example shows that the single-adjoint composite design+adaptation loop, performing the *simultaneous* GO-adaptation and shape improvement, provides a High-Fidelity shape improve-

ment.

Acknowledgements Lemma's NiceFlow-Design project is supported by France 2030 and Next Generation EU and uses HPC resources from GENCI-CINES (Grant 2023-A0142A14070).

Competing Interests The authors have no conflicts of interest to declare that are relevant to the content of this chapter.

Ethics Approval No ethics approval was required.

References

1. A. Dervieux, F. Alauzet, A. Loseille, and B. Koobus. *Mesh adaptation for Computational Fluid Dynamics, tome 1*. ISTE Ltd and John Wiley & Sons, New York (ISBN: 9-781-78630-832-0), 1st edition, 2023.
2. A. Dervieux, F. Alauzet, A. Loseille, and B. Koobus. *Mesh adaptation for Computational Fluid Dynamics, tome 2*. ISTE Ltd and John Wiley & Sons, New York (ISBN: 9-781-78630-832-0), 1st edition, 2023.
3. F. Alauzet and L. Frazza. 3D RANS anisotropic mesh adaptation on the high-lift version of NASA's common research model (HL-CRM). *AIAA paper 2019-2947*, 2020
4. A. Jameson. Aerodynamic design via control theory. *J. Sci. Comput.*, 3:233–260, 1988.
5. J.L. Lions. *Optimal Control of Systems Governed by Partial Differential Equations*. Springer-Verlag, 1971.
6. Y. Mesri, F. Alauzet and A. Dervieux, Coupling optimum shape design and mesh adaptation for sonic boom reduction, *42th CAA-AAAF*, Sophia-Antipolis (F), march 2007
7. O. Pironneau Optimal shape design for aerodynamics. *AGARD REPORT*, 803, 1994.
8. M.A. Park and M. Nemec Near Field Summary and Statistical Analysis of the Second AIAA Sonic Boom Prediction Workshop. 23th AIAA Computational Fluid Dynamics Conference, *AIAA Paper 2017-3256*, Denver, CO, USA, Jun 2017.
9. R. Becker, M. Braack, D. Meidner, R. Rannacher, and B. Vexler. Adaptive finite element methods for PDE-constrained optimal control problems. *Reactive Flows, Diffusion and Transport*, Springer, 2006.
10. L. Frazza, A. Loseille, A. Dervieux, and F. Alauzet. Nonlinear corrector for Reynolds averaged Navier Stokes equations. *Int. J. Numer. Meth. Fluids*, 91(11):567–586, 2019.
11. C.L. Rumsey and J.P. Slotnick. Overview and Summary of the Second AIAA High Lift Prediction Workshop. *Journal of Aircraft*, 52(4):1006–1025, 2015.